HHS Public Access

Author manuscript

J Stroke Cerebrovasc Dis. Author manuscript; available in PMC 2021 September 01.

Published in final edited form as:

J Stroke Cerebrovasc Dis. 2020 September ; 29(9): 104942. doi:10.1016/j.jstrokecerebrovasdis.2020.104942.

Lung SOD3 limits neurovascular reperfusion injury and systemic immune activation following transient global cerebral ischemia.

Nguyen Mai, M.D., Ph.D.[1], **Viollandi Prifti, B.S.**[1], **Kihong Lim, Ph.D.**[3], **Michael A. O'Reilly, Ph.D.**[4], **Minsoo Kim, Ph.D.**[3], **Marc W. Halterman, M.D., Ph.D.**[1,2]

[1]Departments of Neurology, University of Rochester School of Medicine and Dentistry, Rochester NY 14642

[2]Departments of Neuroscience, University of Rochester School of Medicine and Dentistry, Rochester NY 14642

[3]Departments of Microbiology & Immunology, University of Rochester School of Medicine and Dentistry, Rochester NY 14642

[4]Departments of Pediatrics, University of Rochester School of Medicine and Dentistry, Rochester NY 14642

Abstract

Background and Objectives: Studies implicate the lung in moderating systemic immune activation via effects on circulating leukocytes. In this study, we investigated whether targeted expression of the antioxidant extracellular superoxide dismutase (SOD3) within the lung would influence post-ischemic peripheral neutrophil activation and CNS reperfusion injury.

Methods: Adult, male mice expressing human SOD3 within type II pneumocytes were subjected to 15 minutes of transient global cerebral ischemia. Three days post-reperfusion, lung and brain tissue was collected and analyzed by immunohistochemistry for inflammation and injury markers. *In vitro* motility and neurotoxicity assays were conducted to ascertain the direct effects of hSOD3 on PMN activation. Results were compared against C57BL/6 age and sex-matched controls.

Results: Relative to wild-type controls, hSOD3 heterozygous mice exhibited a reduction in lung inflammation, blood-brain barrier damage, and post-ischemic neuronal injury within the hippocampus and cortex. PMNs harvested from hSOD3 mice were also resistant to LPS priming, slower-moving, and less toxic to primary neuronal cultures.

Corresponding Author: Marc W. Halterman, M.D., Ph.D., Departments of Neurology & Neuroscience, University of Rochester Medical Center, 601 Elmwood Avenue, Rochester, NY 14642, Phone: (585) 273-1335, Marc_Halterman@urmc.rochester.edu.

7.0 AUTHOR CONTRIBUTIONS N.M. designed experiments, performed surgical procedures, processed tissues and cells for IHC and flow cytometry, performed *in vitro* experiments, interpreted data, and drafted the initial manuscript. L.P. performed surgical procedures, processed tissues for IHC, and interpreted data. K.L. performed *in vitro* experiments. M.K. and M.O. assisted with experimental design, interpreted data, and reviewed the manuscript. M.W.H. designed experiments, interpreted data, and wrote the final version of the manuscript.

Conclusions: Constitutive, focal expression of hSOD3 is neuroprotective in a model of global cerebral ischemia-reperfusion injury. The underlying mechanism of SOD3-dependent protection is attributable in part to effects on the activation state and toxic potential of circulating neutrophils. These results implicate lung-brain coupling as a determinant of cerebral ischemia- reperfusion injury and highlight post-stroke lung inflammation as a potential therapeutic target in acute ischemic cerebrovascular injuries.

Keywords

Ischemia-reperfusion; global ischemia; neutrophil; superoxide dismutase 3 (SOD3); oxygen glucose deprivation (OGD)

1.0 INTRODUCTION

While polymorphonuclear neutrophils (PMNs) participate in the dissolution and clearance of damaged tissue after ischemic injury, PMNs contribute to post-stroke pathology inducing collateral tissue injury and promoting post-ischemic neuroinflammation[1]. PMN toxicity arises in part through the production and release of reactive oxygen species (ROS) and degradative enzymes[2], and PMN burden in the post-ischemic CNS correlates with poor outcomes after stroke and cardiac arrest[3–7]. Unexpectedly, targeting PMNs proved ineffective in acute ischemic stroke trials leading some to consider PMN infiltration as a surrogate for injury rather than a *bona fide* therapeutic target[8–11]. However, strategies predicated on the global inhibition of PMN function fail to account for the fact that, like macrophages, PMNs can also serve an anti-inflammatory function[12,13]. For example, in a model of focal stroke, neuroprotection conveyed by the PPAR-γ antagonist rosiglitazone was associated with increased infiltration of anti-inflammatory PMNs within the ischemic core and enhanced PMN clearance by microglia[14]. While immune ablative strategies seem not to provide the way forward, studies geared towards modulating the peripheral cues required for innate immune priming could prove advantageous.

Upon release from the bone marrow, circulating PMNs transition from a quiescent to a primed state in response to a pathologic insult. Priming heightens PMN sensitivity to chemotactic cues without triggering NADPH oxidase activity, degranulation, or other potentially cytotoxic responses[15]. This step function protects the host from aberrant PMN activation, and evidence suggesting that priming may be reversible under select conditions[16]. Priming also reduces PMN deformability and capillary transit time[17], which in the pulmonary circulation, increases PMN transmigration into the lung parenchyma[18]. This ‘catch and release’ model mediated by the lung is proposed to protect downstream tissues from errant PMN activation[19,20]. Conversely, under conditions including sepsis and ischemia-reperfusion injury, the intrinsic capacity of the lung to constrain peripheral immune priming is lost[20–22].

The antioxidant extracellular superoxide dismutase (SOD3) is expressed by multiple cell types within the lung where it counteracts the damaging effects of inflammation and fibrosis[23,24]. As a family, the SODs are distinguishable based on their ability to coordinate Cu/Zn (SOD1/3) or manganese (SOD2) and their localization within the cytosol (SOD1),

mitochondria (SOD2), or extracellular matrix (SOD3)[25]. However, all SODs share the ability to convert superoxide radicals to molecular oxygen and hydrogen peroxide, providing tissues the means to defend against the potential toxic effects of inspired oxygen and other sources free radicals. As such, the SODs participate in a range of critical homeostatic and disease-related processes, including cardiovascular development and the tissue response to ischemic injury[25–27]. SOD3 is particularly unique in that it is expressed predominantly in the lung, kidney, and vasculature, where it mitigates free radical damage by initiating the conversion of oxygen radicals to lesser intermediates[28]. Studies indicate that the R213G SOD3 polymorphism, which results in reduced tissue retention through altered c-terminal processing, is associated with premature aging in mice and a doubling of cardiovascular risk in humans[29,30].

In light of recent reports citing acute stroke as a proximate cause of lung inflammation[31], we asked whether these changes contribute to post-ischemic neurodegeneration via effects on systemic immune priming. Specifically, we tested whether expression of human SOD3 (hSOD3) within type II pneumocytes would induce remote ischemic neuroprotection. Using a model of transient global cerebral ischemia that includes systemic immune priming with low-dose bacterial lipopolysaccharide[21], we show that SOD3 induces adaptive lung-brain coupling in part by inhibiting post-ischemic innate immune activation.

2.0 MATERIALS AND METHODS

2.1 Animals.

All animal work was performed in keeping with federal guidelines and with approval by the University Committee on Animal Resources. The TgSOD3 mice expressing human SOD3 specifically within type II pneumocytes under control of the surfactant protein-C promoter generated by Folz et al.[32] were obtained from Dr. Michael O'Reilly (University of Rochester). All mice used in this study were male and matched for both age (4–6-months) and weight (30–40 g). hSOD3 mice were carried as heterozygotes and maintained on the C57BL/6 background, with hSOD3 −/− littermates serving as controls.

2.2 Global cerebral ischemia model.

On Day −10, mice underwent basilar artery occlusion (BAO), as described[33]. After recovery on Day 0, mice were allocated to either the 3VO/LPS or SHAM/SAL treatment groups using QuickCalcs (www.graphad.com/quickcalcs/randomize1.cfm). Mice in the 3VO group underwent 15 minutes of transient bilateral common carotid artery occlusion (BCCAO) with controls undergoing sham surgery involving neck dissection without occlusion (Figure 1A). Daily weights and rectal temperatures were recorded (Figure 1B). Three animals of each genotype were assigned to 3VO/LPS, and 2–3 were assigned to SHAM/SAL. Mice in the 3VO/LPS group received a single intraperitoneal (IP) injection of 50 μg/kg LPS (from *E. coli* O111:B4; Sigma-Aldrich, St. Louis, MO) within 15 minutes following reperfusion. Sample sizes were calculated based on observed differences in cortical injury between SHAM/SAL (7.87 ± 1.76%) and 3VO/LPS-treated WT mice (39.79 ± 7.28%) setting α=0.05 and power=0.9[21].

2.3 Western blotting.

Total lung homogenates were prepared in RIPA assay buffer and analyzed by Western blotting using the following antibodies: goat polyclonal human SOD3 antibody, goat polyclonal mouse SOD3 antibody (both 1:500; R&D Systems, Minneapolis, MN), and mouse monoclonal β-actin antibody (1:10000; Sigma). Donkey anti-goat HRP (IgG H&L) antibody was used at 1:2000 for mouse and human SOD3, and donkey anti-mouse HRP (IgG H&L) antibody was used at 1:10000 for β-actin (both Santa Cruz Biotechnology, Dallas, TX). Membranes were developed using Radiance ECL chemiluminescent HRP substrate per product protocol (Azure Biosystems, Dublin, CA) and imaged on the Azure 600 (Azure Biosystems).

2.4 Flow cytometry.

Retro-orbital blood was collected 2 hours after SAL or LPS injection. Whole blood was washed and lysed with red cell lysis buffer (Biolegend, San Diego, CA) for 5 minutes. Cells were stained for 30 minutes at 4°C with Brilliant Violet 421-labeled anti-Ly-6G (1 μg/ml) and Alexa Fluor 647-labeled anti-CD11b antibodies (0.8 μg/ml) (both Biolegend) with 4 μL Fc receptor block per sample (BD Biosciences, San Jose, CA). Cells were later fixed in 2% paraformaldehyde for 30 minutes[34], and fluorescence was measured using a BD LSR II Flow Cytometer (BD Biosciences). Data were collected for 10,000 events. Forward *vs.* side scatter plots (FSC-area *vs.* SSC-area) were used to identify white blood cells and exclude cell debris. Gates were then manually drawn on plots of FSC-height *vs.* FSC-area plots to gate for single cells. Two-dimensional plots of Ly-6G *vs.* CD11b were used to identity Ly-6G^{hi}/CD11b^{hi} PMNs, and histograms were constructed for each PMN population. Geometric mean fluorescence intensity (MFI) analyses were performed using FlowJo analysis software (TreeStar, Ashland, OR).

2.5 Immunohistochemistry and Image Analyses.

Following intracardiac perfusion and inflation-fixation of the lungs, tissues were removed, post-fixed in 4% paraformaldehyde (Sigma), cut into 25 μm sections using a Leica SM2010R microtome (Leica Biosystems, Buffalo Grove, IL), and stored at 4°C in cryoprotectant. Sections were washed with PBS and blocked in 10% goat serum for 1 hour at 20°C before immunohistochemical (IHC) staining using dilutions as listed (Table S1). Hoechst 3342 and mouse monoclonal anti-MAP2 antibody were obtained from Sigma; rat monoclonal anti-Ly-6B antibody, expressed on neutrophils, inflammatory monocytes and activated macrophages, was obtained from Abcam (Cambridge, UK); rabbit polyclonal anti-Iba1 antibody was obtained from Wako (Richmond, VA); rabbit polyclonal anti-platelet endothelial cell adhesion molecule 1 (PECAM-1) was obtained from BD Pharmingen (San Jose, CA); Alexa Fluor 488 goat anti-mouse IgG (H+L), Alexa Fluor 488 goat anti-rabbit IgG (H+L), and Alexa Fluor 594 goat anti-rat IgG (H+L) were obtained from Life Technologies (Grand Island, NY); DyLight 405 AffiniPure goat anti-mouse IgG was obtained from Jackson ImmunoResearch (West Grove, PA). Sections were imaged using an OptiGrid Structured-Light Imaging System (Qioptiq, Fairport, NY). Investigators were blinded to sample assignments by using an alphanumeric coding strategy. Images were pseudocolored after analyses for consistent presentation of cell types.

Lung total cellularity was measured by counting Hoechst-labeled nuclei in 5 compressed *Z*-stack images per animal. PMN/macrophage infiltration was estimated by measurement of Ly-6B mean gray value in 10 random sections. Alveolar wall thickness was measured as the smallest orthogonal distance between 2 adjacent alveoli. Images for lung quantifications were acquired at 40× magnification using identical settings and values to minimize variability and analyzed using ImageJ (http://rsb.info.nih.gov/ij/).

Loss of microtubule-associated protein 2 (MAP2) staining was used as a surrogate marker for ischemic cortical injury as reported[35,36]. CA1 pyknosis was measured by quantifying ischemia-induced nuclear condensation[37]. Neuronal nuclear area was measured by acquiring *Z*-stack images of CA1 in matched bregma sections at 40x magnification. The outer edges of ≥300 Hoechst-labeled nuclei were traced per animal, and nuclear area was measured using ImageJ. Skeleton analysis of MAP2(+) neurite branching and injury was completed using 2× images of the dentate gyrus hilus from each animal[38]. Images were made binary, skeletonized, and quantified using the Analyze Skeleton plugin in ImageJ[39]. Branch length was defined as the sum of all voxels in each branch. Fluorescence intensity data were calculated from images taken from 5–8 matched, non-contiguous coronal sections spanning +1.70 to −2.92 mm from bregma. PECAM-1 upregulation and IgG leakage were measured by mean gray values (fluorescence intensity) from 4 random cortical sections imaged at 20× magnification per mouse. IgG intensity was normalized to PECAM-1(+) vessel length.

2.6 In vivo neutrophil priming & purification.

Bone marrow cells were harvested from femurs and tibias of WT and TgSOD3 mice in HBSS and incubated with red cell lysis buffer (Biolegend) for 2 minutes. White blood cells were incubated with a PMN biotin-antibody cocktail and anti-biotin microbeads prior to magnetic separation and negative selection per manufacturer instructions (Miltenyi Biotec, Bergisch Gladbach, Germany). For experiments involving primed and unprimed PMNs, mice were injected with either saline (SAL) or 50 μg/kg IP lipopolysaccharide (LPS; Sigma), respectively, 6 hours before bone marrow harvest. We have previously characterized this dose of LPS is sufficient to induce transient PMN activation without inducing significant weight loss, fever, or behavioral change in the host[21].

2.7 Neutrophil migration assays.

WT and TgSOD3 PMNs were harvested from saline- or LPS-injected mice (SAL-PMN, LPS-PMN) and cultured in L-15 media (Thermo Fisher Scientific) supplemented with 4.5 g/L glucose on glass chamber slides coated with 5 μg/ml fibronectin (Sigma). PMNs were stimulated with 1 μM in PBS of the chemoattractant N-formylmethionineleucyl-phenylalanine (fMLP; Sigma) to induce motility[40,41] and allowed to settle for 12 minutes before imaging. Images were acquired every 15 seconds for 20 minutes, and both velocity and directional index for migrating cells were analyzed with Volocity software (PerkinElmer, Waltham, MA). A directional index of 1 indicated movement in a straight line while an index of 0 indicated no displacement from the original position. All steps for migration assays were performed at 37°C. Bright-field live cell movies were acquired at a frame rate of 12 images/minute for a total of 24 hours to assess for PMN uropod formation in co-cultures. PMNs were identified by their spheroid shape and high contrast ratio, and

individual cells were monitored for the extension of one or more uropods during the entire acquisition period. Data were gathered from mixed cultures of OGD-exposed cortical neurons (4 hours) and SAL- or LPS-stimulated PMNs harvested from WT and TgSOD3 mice.

2.8 Neuron-PMN co-cultures.

Cortical neurons were generated as described[42]. Briefly, cortical neurons were dissociated from E15–17 rat embryos and cultured in serum-free Neurobasal media supplemented with L-glutamine and B27 without antioxidants (Thermo Fisher Scientific). Neurons were plated on poly-l-lysine-coated plastic (5000 cells/well in 96-well plates or 30,000 cells/well in 24-well plates) and used between DIV 7–8. 5-Fluoro-2'-deoxyuridine (Sigma-Aldrich, St. Louis, MO) was added at DIV 3 to inhibit the growth of non-neuronal cells. With this method, 99% neuronal purity was achieved at DIV 7 (data not shown). OGD was achieved by replacing culture media with HBSS and incubating cells at 0.5% O_2 in an oxygen control glove box for 4 hours (Coy Laboratory Products, Grass Lake, MI). For reperfusion, HBSS was replaced with conditioned media consisting of 50% fresh and 50% conditioned Neurobasal media removed at the onset of OGD. Neuron cultures were incubated an additional 24 hours prior to analysis. To assess PMN-induced neuron death, WT and TgSOD3 PMNs were harvested from saline- or LPS-injected mice and added 4:1 to normoxic neurons for 24 hours and to 4-hour OGD neurons at the start of 24-hour reperfusion. Movies of co-culture wells were acquired on the Zeiss AxioObserver Z1 microscope at a frame rate of 12 images/minute for 24 hours. Neuron death was defined by somal swelling and rupture and quantified by visual inspection of each frame[43].

2.10 Statistical analyses.

Statistical analyses were performed using Prism (Graphpad, La Jolla, CA). Comparisons were made using 2-way ANOVA and Holm-Sidak post-hoc test for *in vitro* PMN migration assays, uropod count, and neuron death during co-culture, as well as *in vivo* comparisons of lung cellularity, Ly-6B fluorescence, alveolar wall thickness, cortical PMN accumulation, CA1 nuclear area, hippocampal MAP2 fluorescence, DG neurite length, cortical injury, Iba1 fluorescence, PECAM-1 fluorescence, and IgG leakage. Repeated measures ANOVA and Holm-Sidak post-hoc test was used for changes in weight and temperature over time. P values less than 0.05 were considered significant. In all cases, the investigator conducting quantitative image analyses was blinded to the background genotype and treatment arm by coding both video sequences, slides and representative images.

3.0 RESULTS

3.1 hSOD3 lung expression protects against 3VO/LPS-induced lung injury.

To investigate the role of lung inflammation on cerebral reperfusion injury, we used a model of ischemia-reperfusion that combines the immune priming effects of damage-associated molecules released following transient global ischemia with LPS-induced systemic inflammation[21]. Mice were randomized into SHAM/SAL and 3VO/LPS groups with LPS delivered by IP injection following cerebral reperfusion (Figure 1A). Daily post-operative monitoring revealed an effect of the 3VO/LPS procedure on weight but not core temperature,

and no between-strain differences were observed (Figure 1B). To attenuate inflammatory changes intrinsic to the lung, we utilized TgSOD3 mice expressing human *SOD3* under the surfactant protein-C promoter[32]. Western analyses confirmed the expression of the human SOD3 in lung lysates from the transgenic strain and endogenous mouse SOD3 in both lines (Figure 1C). We have previously shown that hSOD3 limits PMN activation in response to 3VO-induced ischemia alone[44]. Consistent with these results, flow analyses confirmed that focal SOD3 expression within the lung in TgSOD3 mice reduced expression of the activation marker CD11b relative to WT controls (TgSOD3 MFI: 25,906 *vs.* WT MFI: 45,064 for 10,000 events) in response to combined 3VO/LPS treatment (Figure 1D).

In light of recent reports citing acute stroke as a proximate cause for lung inflammation[31], we next asked whether targeted SOD3 expression in the TgSOD3 line would prove beneficial. 3VO/LPS increased lung parenchymal cellularity in WT mice ($11.5 \times 10^5 \pm 1.1 \times 10^5$ nuclei/cm^2 *vs.* SHAM/SAL, $8.7 \times 10^5 \pm 0.3 \times 10^5$ nuclei/cm^2; $p = 0.03$), while this effect was inhibited in the TgSOD3 mice undergoing 3VO/LPS ($8.5 \times 10^5 \pm 1.1 \times 10^5$ nuclei/cm^2 *vs.* SHAM/SAL, $8.6 \times 10^5 \pm 0.5 \times 10^5$ nuclei/cm^2; $p = 0.98$). Likewise, 3VO/LPS induced infiltration of Ly-6B(+) neutrophils and inflammatory monocytes in the lungs of WT mice (110.1 ± 43.2 AU *vs.* SHAM/SAL, 19.0 ± 6.7 AU; $p = 0.029$). Again, this effect was ameliorated in the TgSOD3 mice undergoing 3VO/LPS (31.0 ± 27.0 AU *vs.* SHAM/SAL, 18.9 ± 2.9 AU; $p = 0.94$). TgSOD3 expression also reduced alveolar wall thickening (9.0 ± 1.9 μm *vs.* WT, 13.9 ± 1.1 μm; $p = 0.012$) in mice treated with the 3VO/LPS procedure.

3.2 Lung SOD3 modulates ischemia-induced neurovascular injury and inflammation.

Given the observed effects of SOD3 overexpression on markers of peripheral inflammation, we postulated that TgSOD3 mice would also be less susceptible to post-ischemic neurodegeneration and the effects of ischemia-reperfusion injury. We first analyzed the extent of injury observed in the ischemia-sensitive hippocampus (Figure 3). Three days after 3VO/LPS, ischemic injury as observed in the hippocampus of WT mice with pyknosis of CA1 pyramidal cells. Mean nuclear area in 3VO/LPS-treated WT mice (46.8 ± 9.1 μm^2) was diminished compared to that of SHAM/SAL-treated WT animals (63.3 ± 4.5 μm^2; $p = 0.045$) and to 3VO/LPS-treated TgSOD3 mice (63.3 ± 1.1 μm^2; $p = 0.045$) (Figure 3A–B). We also observed loss of MAP2 signal within the CA1 neuritic field (3VO/LPS, 112.7 ± 91.0 AU *vs.* SHAM/SAL, 455.9 ± 43.6 AU; $p = 0.001$) of WT mice (Figure 3A & C). While this area was also injured in TgSOD3 mice (3VO/LPS, 244.9 ± 23.4 AU *vs.* SHAM/SAL, 480.4 ± 24.5 AU; $p = 0.01$), the effect was mitigated relative to WT ($p = 0.047$). Dendritic branch length was also reduced in the hilus of the dentate gyrus in WT mice following 3VO/LPS treatment (0.4 ± 0.1 μm/μm^2 *vs.* SHAM/SAL, 0.7 ± 0.1 μm/μm^2; $p = 0.045$), an effect not observed in TgSOD3 mice (3VO/LPS, 0.8 ± 0.1 μm/μm^2 *vs.* SHAM/SAL, 0.7 ± 0.0 μm/μm^2; $p = 0.63$) (Figure 3D–E).

TgSOD3 mice also exhibited less cortical damage based on the area of MAP2 signal loss (20.7 ± 3.8%) compared to WT mice (39.9 ± 10.9%; $p = 0.025$) (Figure 4A–B). Of note, hSOD3-dependent neuroprotection was associated with a non-significant reduction in the number of Ly-6B(+) cortical neutrophils and inflammatory macrophages (WT, 944.2 ±

489.0 PMN/cm^2 *vs.* TgSOD3, 368.2 ± 441.7 PMN/cm^2; $p = 0.31$), though 3VO/LPS induced PMN infiltration well above that observed in SHAM/SAL controls [$F(1,7) = 6.26$; $p = 0.041$].TgSOD3 mice were, however, protected from cerebrovascular reperfusion injury (Figure 4A, C-D). While 3VO/LPS increased expression of the endothelial activation marker PECAM-1 in WT mice (38.2 ± 11.1 AU *vs.* SHAM/SAL, 7.3 ± 1.2 AU; $p = 0.005$), TgSOD3 mice undergoing 3VO/LPS were protected against this effect (17.5 ± 6.0 AU; $p = 0.029$ *vs.* WT). In addition, TgSOD3 mice were protected against 3VO/LPS-induced BBB leak (4.0 ± 0.6 AU) compared to WT (7.0 ± 1.5 AU; $p = 0.02$) using IgG interstitial leakage as a surrogate marker. TgSOD3 expression was also associated with a reduction in cortical levels of the microglial activation marker Iba1 (243.9 ± 116.7 AU) following 3VO/LPS relative to wild type controls (529.2 ± 101.5 AU; $p = 0.019$) (Figure 4 A, E).

3.3 PMNs derived from TgSOD3 mice are phenotypically distinct.

Given the observed effect of lung-directed hSOD3 overexpression on the activation state of circulating PMNs, we next asked whether PMNs collected from TgSOD3 and WT mice were phenotypically different. To induce PMN priming, mice received either saline or low-dose LPS by IP injection prior to harvesting to induce systemic inflammation (Figure 5A). We have shown that 50 μg/kg IP LPS is sufficient to induce CD11b expression on PMNs without influencing peripheral WBC counts, temperature, or weight in WT mice[21]. After negative immunoaffinity selection, flow cytometry using the PMN marker Ly-6G (clone 1A8) and the surface activation marker CD11b confirmed LPS-induced PMN activation (Figure 5B). Since LPS also induces formyl peptide receptors that mediate PMN chemotactic responses to fMLP[40], we asked whether PMNs harvested from saline- and LPS-injected mice would respond differently to fMLP induced migration *in vitro*. Plates were also coated with fibronectin, which is prevalent in brain parenchyma, migration-inducing, and upregulated after stroke (Figure 5C)[45]. Results show that stimulation with 1 μM fMLP, PMNs from both SAL and LPS-treated TgSOD3 mice traveled at lower velocities compared to WT SAL-PMNs on fibronectin [$F(1,50) = 13.6$; $p = 0.0006$]. WT LPS-PMN traveled at lower velocity (0.1 ± 0.0 μm/s *vs.* 0.2 ± 0.1 μm/s; $p = 0.002$) than WT SAL-PMNs, though the effect of LPS stimulation was not observed in TgSOD3 PMNs. TgSOD3 PMNs also had a higher directional index on fibronectin [$F(1,50) = 12.8$; $p = 0.001$], traveling on a direct rather than oscillatory course. Directionality appeared to be a genotype-specific difference that was not affected by LPS [$F(1,50) = 0.62$; $p = 0.44$]. We also cultured PMNs with neurons primed by oxygen-glucose deprivation and tracked the frequency of uropod formation, considered a surrogate marker of PMN motility[46]. Consistent with these observations, TgSOD3-derived PMNs also generated fewer uropods relative to WT PMNs (0.60 ± 0.06 *vs.* WT, 0.42 ± 0.15; $p = 0.0.032$) (Figure 5D).

3.4 PMNs derived from TgSOD3 mice are less toxic to neurons in vitro.

Given the correlation between TgSOD3 status and PMN function, we asked if PMNs harvested from TgSOD3 mice were less toxic to primary neuronal cultures. PMNs were harvested from donor mice 6 hours after a single IP injection of either LPS or saline (Figure 6A). PMNs were added at a 4:1 ratio relative to neurons and analyzed for neuronal rupture after 24 hours by bright field microscopy[43] (Figure 6B). Results indicate that LPS-primed PMNs from WT donors induced significant neuronal injury relative to controls (7.3 ± 1.9%

vs. Ctrl, 3.4 ± 2.0%; $p = 0.025$). Also, two-way ANOVA revealed a significant genotype effect, with TgSOD3 PMNs causing less neuron death overall [$F(1,10) = 5.36$; $p = 0.043$]. We also primed cortical cultures using sub-lethal (4 hours) oxygen-glucose deprivation (OGD) to look for potential synergy with LPS-induced PMN priming. We found that WT LPS-priming enhanced PMN-induced neurotoxicity relative to saline-treated controls (18.5 ± 2.1% vs. 6.2 ± 2.6%; $p < 0.05$) and that PMNs from LPS-primed TgSOD3 donor mice were non-toxic (8.03 ± 3.39%; $p = 0.019$) (Figure 6C & D). And as before, adding PMNs to OGD primed neurons revealed genotype-dependent effects [$F(1,10) = 13.23$; $p = 0.005$].

4.0 DISCUSSION

Systemic innate immune activation contributes to post-stroke behavioral deficits and CNS pathology[47]. In the current study, we show that focal inhibition of oxidant stress in the mouse lung via expression of SOD3 in type II pneumocytes protects against 3VO/LPS-induced lung injury, PMN activation, and brain injury. We also found that PMNs harvested from donor mice expressing human SOD3 within the lung are both phenotypically distinct and non-toxic, despite LPS-induced priming. These studies underscore the pathological role that PMNs serve in reperfusion injury and highlight lung-brain immunological coupling as a novel therapeutic target in acute brain ischemia.

The role PMNs play in the context of cerebral ischemia is multifaceted and context dependent. The extent of PMN activation post-stroke is reflected in part by surface expression of CD11b, which correlates directly with NIH Stroke Scale scores[48]. However, our work underscores the lung's capacity to modulate systemic PMN activation in the context of ischemia-reperfusion injury[20–22]. Specifically, SOD3 released from the lung and kidney moderate tissue injury by limiting the accumulation of free radicals in these tissues and in circulation. While PMNs do not produce *SOD3* mRNA[49], they nonetheless endocytose SOD3 and release it upon stimulation with either fMLP or phorbol 12-myristate 13-acetate (PMA). In this scenario, SOD3 limits PMN activation, the production of TNF-α, IL-1β, and IL-6, and the expression of adhesion molecules, including ICAM-1 and P-selectin on the vascular endothelium[50,51]. Thus, in the context of a SOD3-rich environment, PMNs are less susceptible to activation and could, in theory, modulate inflammation via the release of SOD3 at remote sites[49].

PMNs harvested from WT and TgSOD3 donors were also phenotypically unique in several respects. First, PMNs exposed to hSOD3 exhibited reduced basal velocity *in vitro*. fMLP stimulation also yielded a high directional index (lower path tortuosity) for TgSOD3 PMN migration plated on the extracellular matrix component fibronectin. At the same time, PMNs from WT mice exhibited more back-and-forth motion. This was accompanied by the propensity for PMNs from TgSOD3 mice to generate fewer uropods *in vitro*, reflective of reduced motility and fewer contacts with neuronal processes. Analyses of time-lapse video co-cultures also revealed that PMNs made frequent contact with the neuritic arbor as well as the neuronal soma. This is noteworthy since PMNs have been found to migrate to sites of remote post-ischemic neurodegeneration that make synaptic contact within the primary infarct[52].

While models of global cerebral ischemia can provide insights regarding basic mechanisms of post-ischemic cerebral injury, they do not faithfully recapitulate the multiorgan and immune involvement seen following global anoxia, systemic hypotension, or cardiac arrest. Given reports linking serum endotoxin levels with post-cardiac arrest survival, we previously developed the 3VO/LPS model to more accurately mirror the systemic pathology associated with the post-cardiac arrest syndrome (PCAS)[21,53]. Relative to three-vessel occlusion (3VO) alone, low-dose administration of systemic endotoxin induces immune activation without associated CNS damage[21]. Therefore, to explore the adaptive benefit of lung-brain coupling under more stringent conditions, we focused on using the two-hit (3VO/LPS) model. Aside from the direct activation of innate immunity mediated by toll-like receptor signaling, we predicted that systemic endotoxemia would compromise the capacity of the lung to deprime circulating PMNs. And consistent with reports showing the ability of targeted SOD3 expression to inhibit lung injury caused by hyperoxia and other toxicants[54–57], we found TgSOD3 mice exhibited lower levels of peripheral PMN activation, pulmonary cellular infiltrates, and inter-alveolar septal thickening three days post-reperfusion. Remarkably, we also found that the cerebral microvasculature of TgSOD3 mice was resistant to reperfusion damage induced by the 3VO/LPS model. Specifically, TgSOD3 mice exhibited reduced levels of endothelial inflammation, neuroinflammation, and post-ischemic neurodegeneration within the hippocampus and cortex.

While the effects of global overexpression or knockdown of the SOD family on post-stroke outcomes are reported, this work establishes that restricted expression of hSOD3 in the lung is sufficient to induce remote ischemic neuroprotection. We pursued overexpression rather than an SOD3 knock-out due to findings of respiratory distress and death in acute SOD3 knock-outs exposed to ambient air[58]. Further, protection by way of overexpression suggests that other means of SOD3 delivery may also be beneficial, which is interesting in terms of drug delivery mechanisms. Of note, SOD3 expression did not influence post-ischemic PMN transmigration to the CNS to a significant degree in our model. However, the effects on PMN CD11b expression, markers of endothelial injury (i.e., PECAM-1 and IgG leak), microglial activation suggest SOD3 shed from the lung acts by disrupting pathological interactions between the peripheral immune system and cerebrovascular network. Moreover, PMNs harvested from TgSOD3 mice were less toxic to cultured neurons, suggesting that SOD3 induces PMN reprogramming *in vivo*. For example, exposure to hSOD3 may serve to limit PMN activation and degranulation in response to cues presented by OGD-or 3VO/LPS-injured neurons by modulating the sensitivity of pattern recognition receptors. Further study is required to establish the precise mechanism(s) responsible for constrained PMN activation in the context of ischemia-reperfusion injury.

In summary, these data expand our understanding of and appreciation for the pathological role PMNs play in the setting of CNS ischemia-reperfusion injury. Moreover, our data indicate that SOD3 induces adaptive lung-brain coupling in part by inhibiting post-ischemic innate immune activation. While the exact mechanism responsible for limiting PMN activation in TgSOD3 mice remains unsettled, the SOD3-dependent effects on PMNs are durable, persisting outside the donor mouse. And while we pursued the therapeutic benefits of SOD3 overexpression in the PCAS model, these studies argue that disease states capable of inducing SOD3 dysregulation in the lung could have important effects on both stroke risk

and post-stroke outcomes mediated by elevated levels of innate immune priming during the post-ischemic period.

Supplementary Material

Refer to Web version on PubMed Central for supplementary material.

Acknowledgments

Grant Support: These studies were supported by grants to N.M. (NIH, NS092168) and M.W.H. (NIH, NS092455).

5.0 REFERENCES

1. Jordan JE, Zhao ZQ & Vinten-Johansen J The role of neutrophils in myocardial ischemia-reperfusion injury. Cardiovasc Res 43, 860–878 (1999). [PubMed: 10615413]
2. Barone FC, et al. Reperfusion increases neutrophils and leukotriene B4 receptor binding in rat focal ischemia. Stroke 23, 1337–1347; discussion 1347–1338 (1992). [PubMed: 1381529]
3. Buck BH, et al. Early neutrophilia is associated with volume of ischemic tissue in acute stroke. Stroke 39, 355–360 (2008). [PubMed: 18162626]
4. Segel GB, Halterman MW & Lichtman MA The paradox of the neutrophil's role in tissue injury. J Leukoc Biol 89, 359–372 (2011). [PubMed: 21097697]
5. Wei X, et al. Hydrogen Sulfide Inhalation Improves Neurological Outcome via NF-kappaB-Mediated Inflammatory Pathway in a Rat Model of Cardiac Arrest and Resuscitation. Cell Physiol Biochem 36, 1527–1538 (2015). [PubMed: 26159236]
6. Yune HY, et al. Delta neutrophil index as a promising prognostic marker in out of hospital cardiac arrest. PLoS One 10, e0120677 (2015). [PubMed: 25798609]
7. Maestrini I, et al. Higher neutrophil counts before thrombolysis for cerebral ischemia predict worse outcomes. Neurology 85, 1408–1416 (2015). [PubMed: 26362283]
8. del Zoppo GJ Acute anti-inflammatory approaches to ischemic stroke. Annals of the New York Academy of Sciences 1207, 143–148 (2010). [PubMed: 20955437]
9. Enlimomab Acute Stroke Trial I Use of anti-ICAM-1 therapy in ischemic stroke: results of the Enlimomab Acute Stroke Trial. Neurology 57, 1428–1434 (2001). [PubMed: 11673584]
10. Jickling GC, et al. Targeting neutrophils in ischemic stroke: translational insights from experimental studies. Journal of cerebral blood flow and metabolism : official journal of the International Society of Cerebral Blood Flow and Metabolism 35, 888–901 (2015).
11. Krams M, et al. Acute Stroke Therapy by Inhibition of Neutrophils (ASTIN): an adaptive dose-response study of UK-279,276 in acute ischemic stroke. Stroke 34, 2543–2548 (2003). [PubMed: 14563972]
12. Easton AS Neutrophils and stroke - can neutrophils mitigate disease in the central nervous system? International immunopharmacology 17, 1218–1225 (2013). [PubMed: 23827753]
13. Garcia-Culebras A, et al. Role of TLR4 (Toll-Like Receptor 4) in N1/N2 Neutrophil Programming After Stroke. Stroke 50, 2922–2932 (2019). [PubMed: 31451099]
14. Cuartero MI, et al. N2 neutrophils, novel players in brain inflammation after stroke: modulation by the PPARgamma agonist rosiglitazone. Stroke 44, 3498–3508 (2013). [PubMed: 24135932]
15. Miralda I, Uriarte SM & McLeish KR Multiple Phenotypic Changes Define Neutrophil Priming. Front Cell Infect Microbiol 7, 217 (2017). [PubMed: 28611952]
16. Kitchen E, Rossi AG, Condliffe AM, Haslett C & Chilvers ER Demonstration of reversible priming of human neutrophils using platelet-activating factor. Blood 88, 4330–4337 (1996). [PubMed: 8943870]
17. Lien DC, et al. Physiological neutrophil sequestration in the lung: visual evidence for localization in capillaries. Journal of applied physiology (Bethesda, Md. : 1985) 62, 1236–1243 (1987).
18. Hogg JC & Doerschuk CM Leukocyte traffic in the lung. Annu Rev Physiol 57, 97–114 (1995). [PubMed: 7778886]

19. Summers C, et al. Pulmonary retention of primed neutrophils: a novel protective host response, which is impaired in the acute respiratory distress syndrome. Thorax 69, 623–629 (2014). [PubMed: 24706039]
20. Singh NR, et al. Acute lung injury results from failure of neutrophil de-priming: a new hypothesis. Eur J Clin Invest 42, 1342–1349 (2012). [PubMed: 22984929]
21. Mai N, Prifti L, Rininger A, Bazarian H & Halterman MW Endotoxemia induces lung-brain coupling and multi-organ injury following cerebral ischemia-reperfusion. Exp Neurol 297, 82–91 (2017). [PubMed: 28757259]
22. Roy SK, et al. Chemically modified tetracycline 3 prevents acute respiratory distress syndrome in a porcine model of sepsis + ischemia/reperfusion-induced lung injury. Shock 37, 424–432 (2012). [PubMed: 22258231]
23. Kinnula VL & Crapo JD Superoxide dismutases in the lung and human lung diseases. Am J Respir Crit Care Med 167, 1600–1619 (2003). [PubMed: 12796054]
24. Gulinello M, Lebesgue D, Jover-Mengual T, Zukin RS & Etgen AM Acute and chronic estradiol treatments reduce memory deficits induced by transient global ischemia in female rats. Hormones and behavior 49, 246–260 (2006). [PubMed: 16125703]
25. Fukai T & Ushio-Fukai M Superoxide dismutases: role in redox signaling, vascular function, and diseases. Antioxid Redox Signal 15, 1583–1606 (2011). [PubMed: 21473702]
26. Kawase M, et al. Exacerbation of delayed cell injury after transient global ischemia in mutant mice with CuZn superoxide dismutase deficiency. Stroke 30, 1962–1968 (1999). [PubMed: 10471451]
27. Sugawara T, et al. Overexpression of copper/zinc superoxide dismutase in transgenic rats protects vulnerable neurons against ischemic damage by blocking the mitochondrial pathway of caspase activation. The Journal of neuroscience : the official journal of the Society for Neuroscience 22, 209–217 (2002). [PubMed: 11756504]
28. Oury TD, Day BJ & Crapo JD Extracellular superoxide dismutase in vessels and airways of humans and baboons. Free Radic Biol Med 20, 957–965 (1996). [PubMed: 8743981]
29. Kwon MJ, Lee KY, Lee HW, Kim JH & Kim TY SOD3 Variant, R213G, Altered SOD3 Function, Leading to ROS-Mediated Inflammation and Damage in Multiple Organs of Premature Aging Mice. Antioxid Redox Signal 23, 985–999 (2015). [PubMed: 25927599]
30. Kobylecki CJ, Afzal S & Nordestgaard BG Genetically Low Antioxidant Protection and Risk of Cardiovascular Disease and Heart Failure in Diabetic Subjects. EBioMedicine 2, 2010–2015 (2015). [PubMed: 26844281]
31. Austin V, Ku JM, Miller AA & Vlahos R Ischaemic stroke in mice induces lung inflammation but not acute lung injury. Scientific reports 9, 3622 (2019). [PubMed: 30842652]
32. Folz RJ, Abushamaa AM & Suliman HB Extracellular superoxide dismutase in the airways of transgenic mice reduces inflammation and attenuates lung toxicity following hyperoxia. J Clin Invest 103, 1055–1066 (1999). [PubMed: 10194479]
33. Thal SC, Thal SE & Plesnila N Characterization of a 3-vessel occlusion model for the induction of complete global cerebral ischemia in mice. J Neurosci Methods 192, 219–227 (2010). [PubMed: 20688105]
34. Highland MA, et al. Differences in leukocyte differentiation molecule abundances on domestic sheep (Ovis aries) and bighorn sheep (Ovis canadensis) neutrophils identified by flow cytometry. Comp Immunol Microbiol Infect Dis 46, 40–46 (2016). [PubMed: 27260809]
35. Dawson DA & Hallenbeck JM Acute focal ischemia-induced alterations in MAP2 immunostaining: description of temporal changes and utilization as a marker for volumetric assessment of acute brain injury. Journal of cerebral blood flow and metabolism : official journal of the International Society of Cerebral Blood Flow and Metabolism 16, 170–174 (1996).
36. Kitagawa K, et al. Microtubule-associated protein 2 as a sensitive marker for cerebral ischemic damage--immunohistochemical investigation of dendritic damage. Neuroscience 31, 401–411 (1989). [PubMed: 2797444]
37. Rininger A, Wayland A, Prifti V & Halterman MW Assessment of CA1 injury after global ischemia using supervised 2D analyses of nuclear pyknosis. J Neurosci Methods 207, 181–188 (2012). [PubMed: 22542732]

38. Buczynski BW, et al. Lung-Specific Extracellular Superoxide Dismutase Improves Cognition of Adult Mice Exposed to Neonatal Hyperoxia. Frontiers in medicine 5, 334 (2018). [PubMed: 30619855]
39. Arganda-Carreras I, Fernandez-Gonzalez R, Munoz-Barrutia A & Ortiz-De-Solorzano C 3D reconstruction of histological sections: Application to mammary gland tissue. Microsc Res Tech 73, 1019–1029 (2010). [PubMed: 20232465]
40. Wang X, Qin W, Zhang Y, Zhang H & Sun B Endotoxin promotes neutrophil hierarchical chemotaxis via the p38-membrane receptor pathway. Oncotarget 7, 74247–74258 (2016). [PubMed: 27655676]
41. Ebrahimzadeh PR, Hogfors C & Braide M Neutrophil chemotaxis in moving gradients of fMLP. J Leukoc Biol 67, 651–661 (2000). [PubMed: 10811005]
42. Perry SW, Norman JP, Litzburg A & Gelbard HA Antioxidants are required during the early critical period, but not later, for neuronal survival. J Neurosci Res 78, 485–492 (2004). [PubMed: 15389829]
43. Li D, Shao Z, Vanden Hoek TL & Brorson JR Reperfusion accelerates acute neuronal death induced by simulated ischemia. Exp Neurol 206, 280–287 (2007). [PubMed: 17599834]
44. Mai N, et al. Lung-Derived SOD3 Attenuates Neurovascular Injury After Transient Global Cerebral Ischemia. Journal of the American Heart Association 8, e011801 (2019). [PubMed: 31030600]
45. Howe MD, et al. Fibronectin induces the perivascular deposition of cerebrospinal fluid-derived amyloid-beta in aging and after stroke. Neurobiology of aging 72, 1–13 (2018). [PubMed: 30172921]
46. Hind LE, Vincent WJ & Huttenlocher A Leading from the Back: The Role of the Uropod in Neutrophil Polarization and Migration. Developmental cell 38, 161–169 (2016). [PubMed: 27459068]
47. Neumann J, et al. Very-late-antigen-4 (VLA-4)-mediated brain invasion by neutrophils leads to interactions with microglia, increased ischemic injury and impaired behavior in experimental stroke. Acta Neuropathol 129, 259–277 (2015). [PubMed: 25391494]
48. Weisenburger-Lile D, et al. Harmful neutrophil subsets in patients with ischemic stroke: Association with disease severity. Neurol Neuroimmunol Neuroinflamm 6, e571 (2019). [PubMed: 31355307]
49. Iversen MB, et al. Extracellular superoxide dismutase is present in secretory vesicles of human neutrophils and released upon stimulation. Free Radic Biol Med 97, 478–488 (2016). [PubMed: 27394172]
50. Salvemini D, et al. Pharmacological manipulation of the inflammatory cascade by the superoxide dismutase mimetic, M40403. Br J Pharmacol 132, 815–827 (2001). [PubMed: 11181422]
51. Salvemini D, Riley DP & Cuzzocrea S SOD mimetics are coming of age. Nat Rev Drug Discov 1, 367–374 (2002). [PubMed: 12120412]
52. Jones KA, et al. Peripheral immune cells infiltrate into sites of secondary neurodegeneration after ischemic stroke. Brain Behav Immun 67, 299–307 (2018). [PubMed: 28911981]
53. Grimaldi D, et al. High Level of Endotoxemia Following Out-of-Hospital Cardiac Arrest Is Associated With Severity and Duration of Postcardiac Arrest Shock. Crit Care Med 43, 2597–2604 (2015). [PubMed: 26427593]
54. Buczynski BW, Yee M, Martin KC, Lawrence BP & O'Reilly MA Neonatal hyperoxia alters the host response to influenza A virus infection in adult mice through multiple pathways. Am J Physiol Lung Cell Mol Physiol 305, L282–290 (2013). [PubMed: 23748535]
55. Ghio AJ, Suliman HB, Carter JD, Abushamaa AM & Folz RJ Overexpression of extracellular superoxide dismutase decreases lung injury after exposure to oil fly ash. Am J Physiol Lung Cell Mol Physiol 283, L211–218 (2002). [PubMed: 12060579]
56. Poonyagariyagorn HK, et al. Superoxide dismutase 3 dysregulation in a murine model of neonatal lung injury. Am J Respir Cell Mol Biol 51, 380–390 (2014). [PubMed: 24673633]
57. Van Rheen Z, et al. Lung extracellular superoxide dismutase overexpression lessens bleomycin-induced pulmonary hypertension and vascular remodeling. Am J Respir Cell Mol Biol 44, 500–508 (2011). [PubMed: 20539010]

58. Gongora MC, et al. Loss of extracellular superoxide dismutase leads to acute lung damage in the presence of ambient air: a potential mechanism underlying adult respiratory distress syndrome. Am J Pathol 173, 915–926 (2008). [PubMed: 18787098]

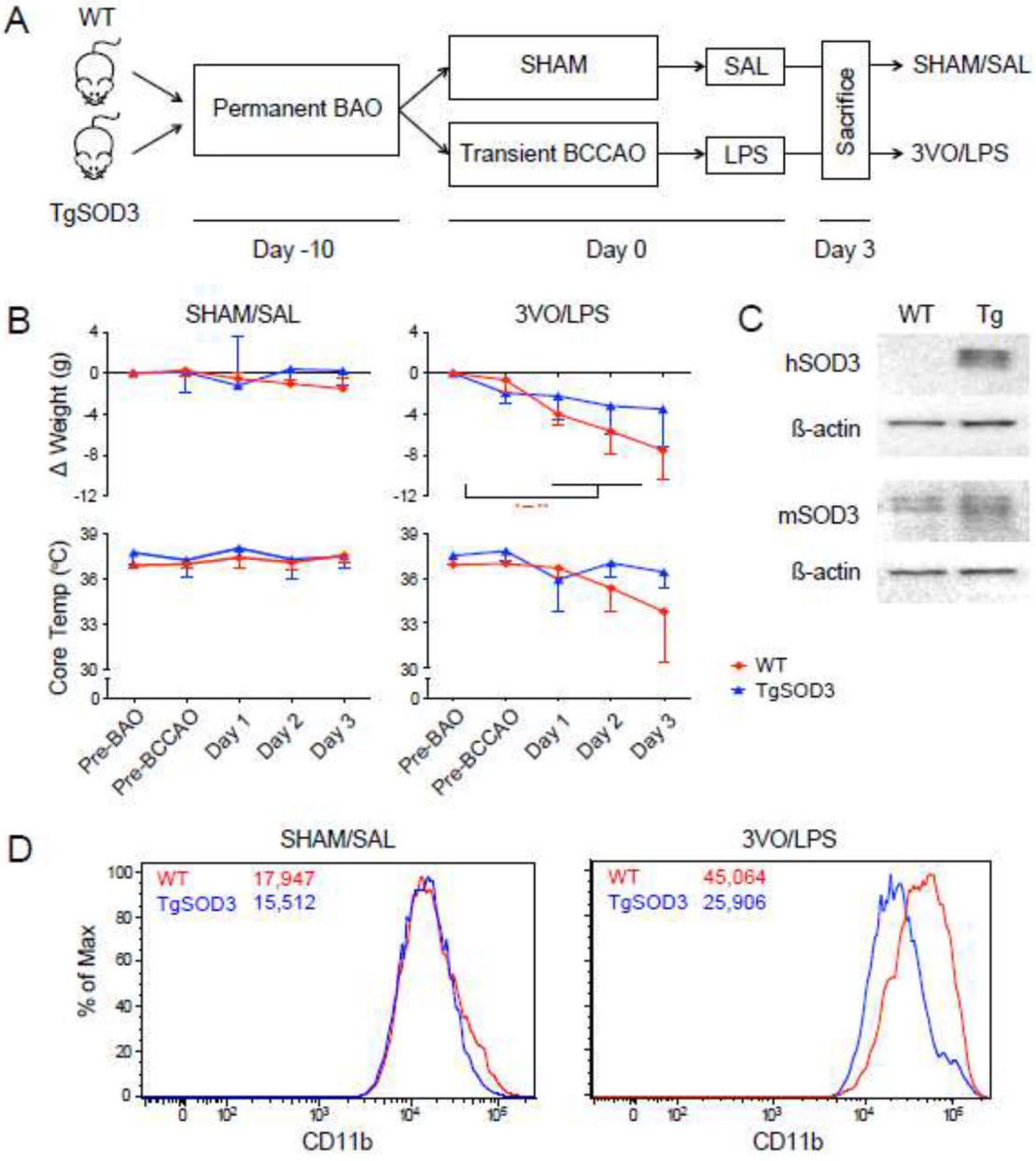

Figure 1.

Study design and physiological parameters. (A) Adult male WT and TgSOD3 mice were randomized to SHAM/SAL and 3VO/LPS treatment groups. Ten days following permanent basilar artery occlusion (BAO), animals underwent either sham surgery followed by saline injection (SHAM/SAL) or 15-minute bilateral common carotid artery occlusion (BCCAO) followed by LPS injection (3VO/LPS). Animals were sacrificed after 3 days. (B) Changes in weight and core temperature caused by SHAM/SAL vs. 3VO/LPS treatment. Values represent means ± SD (n = 4–7). * $p < 0.05$, ** $p < 0.01$ compared to pre-BAO values. (C) Western blot showing human SOD3 (hSOD3) expression in TgSOD3 lungs and mouse SOD3 (mSOD3) expression in both WT and TgSOD3 lungs. (D) Selective hSOD3 expression in the lung mitigates PMN activation caused by 3VO/LPS. Mean fluorescence

intensity of surface CD11b on Ly-6G^{hi}/CD11b^{hi} PMNs 2 hours after SHAM/SAL and 3VO/LPS.

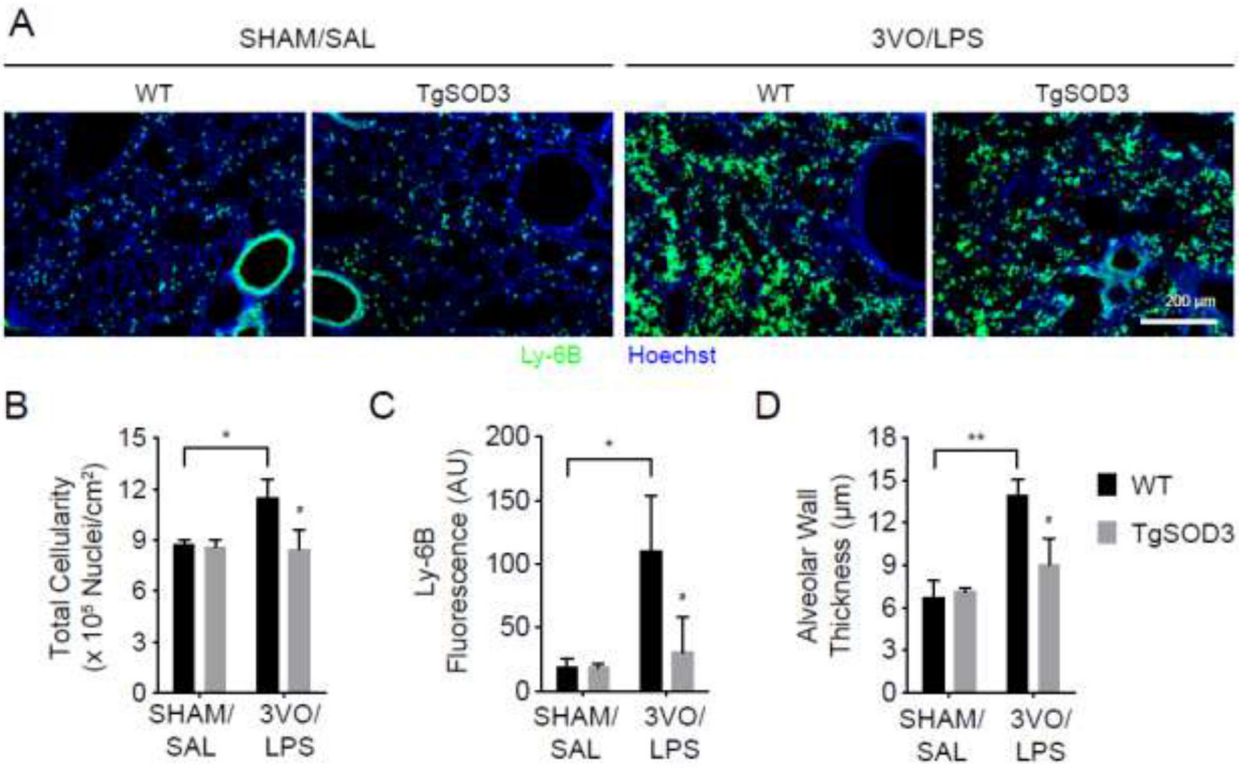

Figure 2.

Lungs from TgSOD3 mice are protected against 3VO/LPS-induced injury. (A) Representative micrographs of WT and TgSOD3 lungs demonstrating the infiltration of Ly-6B(+) PMNs and macrophages (green) 3 days following SHAM/SAL or 3VO/LPS. (B-D) Differences in total cellularity, immune infiltrates (Ly-6B fluorescence), and alveolar wall thickness between WT and TgSOD3 mice are shown. Values represent means ± SD (n = 4–7). * $p < 0.05$, ** $p < 0.01$ between SHAM/SAL and 3VO/LPS; $^{\#}$ $p < 0.05$ between WT and TgSOD3.

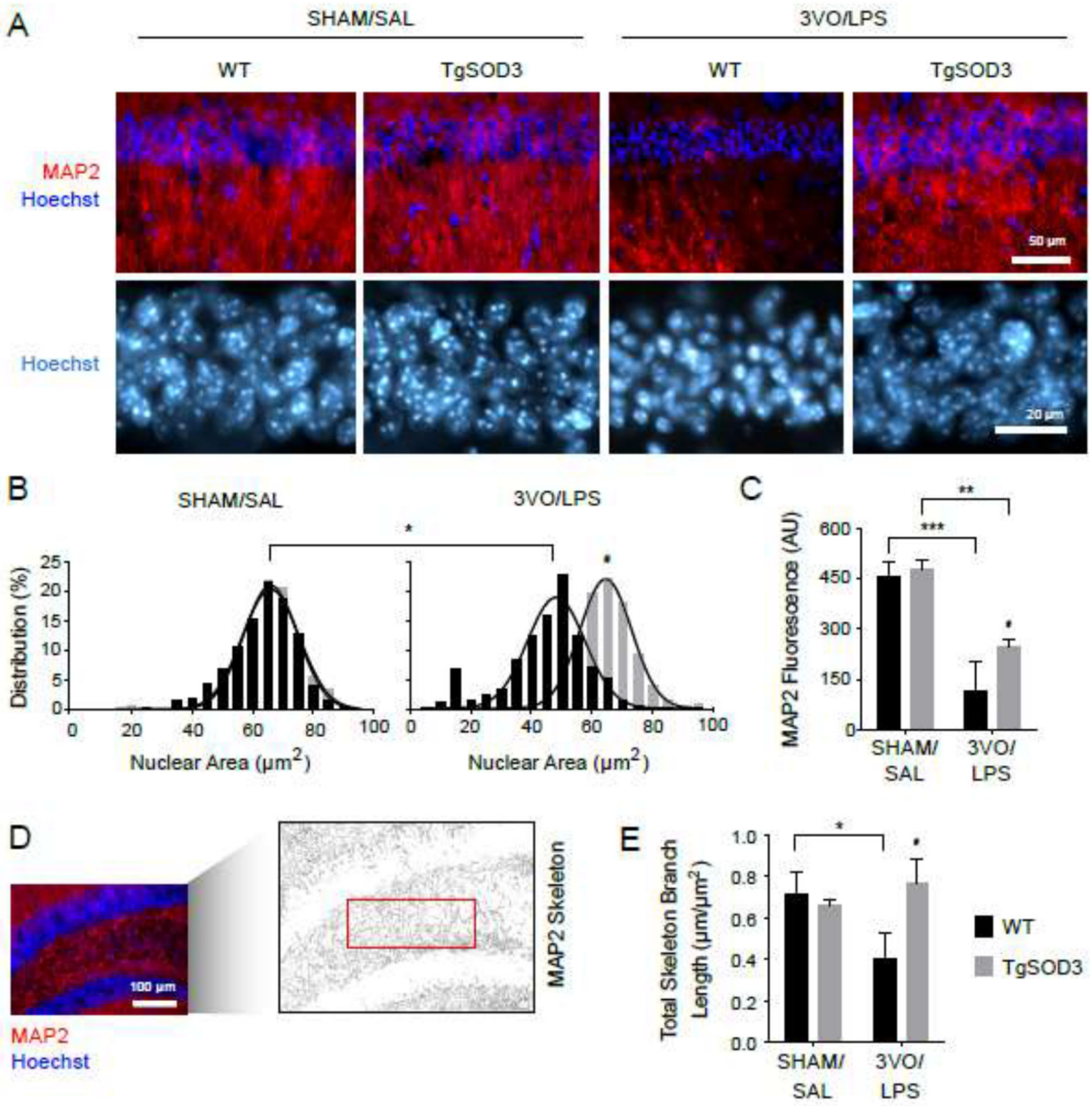

Figure 3.

TgSOD3 mice are protected against post-ischemic hippocampal injury. (A) IHC analyses of 3VO/LPS-induced hippocampal injury in both WT and TgSOD3 mice three days post-reperfusion. IHC analyses of CA1 from WT and TgSOD3 mice reveal neuritic injury with loss of MAP2 staining (red) in the stratum radiatum and the condensation of neuronal nuclei (Hoechst, blue) in the stratum pyramidale. (B) Quantification of neuronal pyknosis within CA1 in WT and TgSOD3 mice with frequency distribution of nuclear size in WT and TgSOD3 mice exposed to SHAM/SAL and 3VO/LPS conditions. (C) Quantification of MAP2 fluorescence intensity in the stratum radiatum. (D-E) Skeletonization of MAP2(+) fibers in the hilus of the dentate gyrus and changes in branch density following SHAM/SAL

or 3VO/LPS. Values represent means ± SD (n = 4–7). * $p < 0.05$, ** $p < 0.01$, *** $p < 0.001$ between SHAM/SAL and 3VO/LPS; $^{\#}$ $p < 0.05$ between WT and TgSOD3.

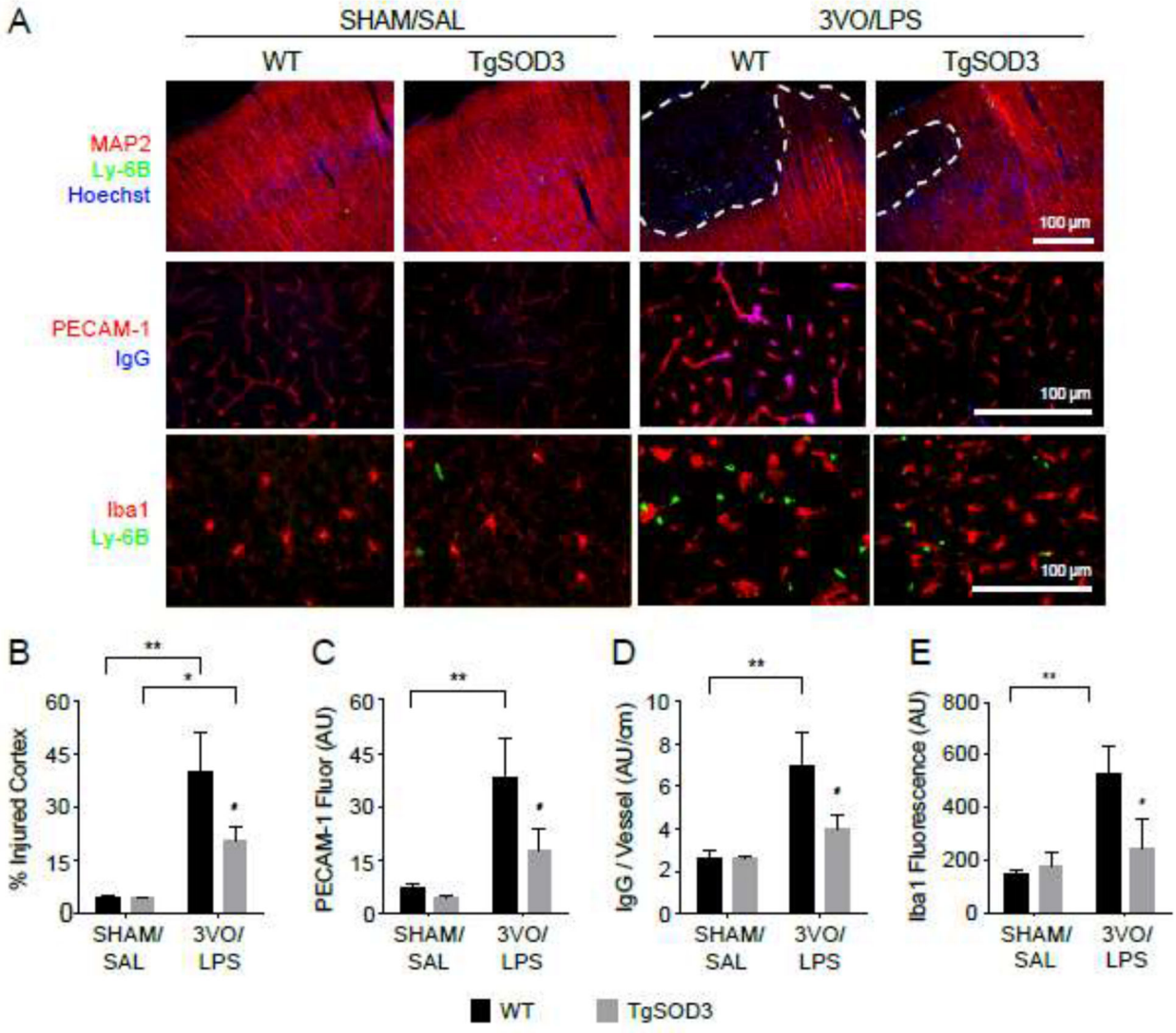

Figure 4.

TgSOD3 mice are protected against 3VO/LPS-mediated cortical injury. (A) IHC analyses of neuronal injury (MAP2, red) and PMN infiltration (Ly-6B, green) (top); vascular PECAM-1 upregulation (red) with perivascular IgG deposition (blue) (middle); and microglial Iba1 upregulation (red) (bottom) in WT and TgSOD3 mice 3 days following 3VO/LPS. (B) Histogram demonstrating cortical injury denoted percent area of MAP2 signal attenuation. (C-D) TgSOD3 effects on vascular PECAM-1 upregulation and extravasation of mouse IgG across the blood-brain barrier. (E) TgSOD3 effects on microglial activation as measured by Iba1 upregulation. Values represent means ± SD (n = 4–7). * $p < 0.05$, ** $p < 0.01$ between SHAM/SAL and 3VO/LPS; # $p < 0.05$ between WT and TgSOD3.

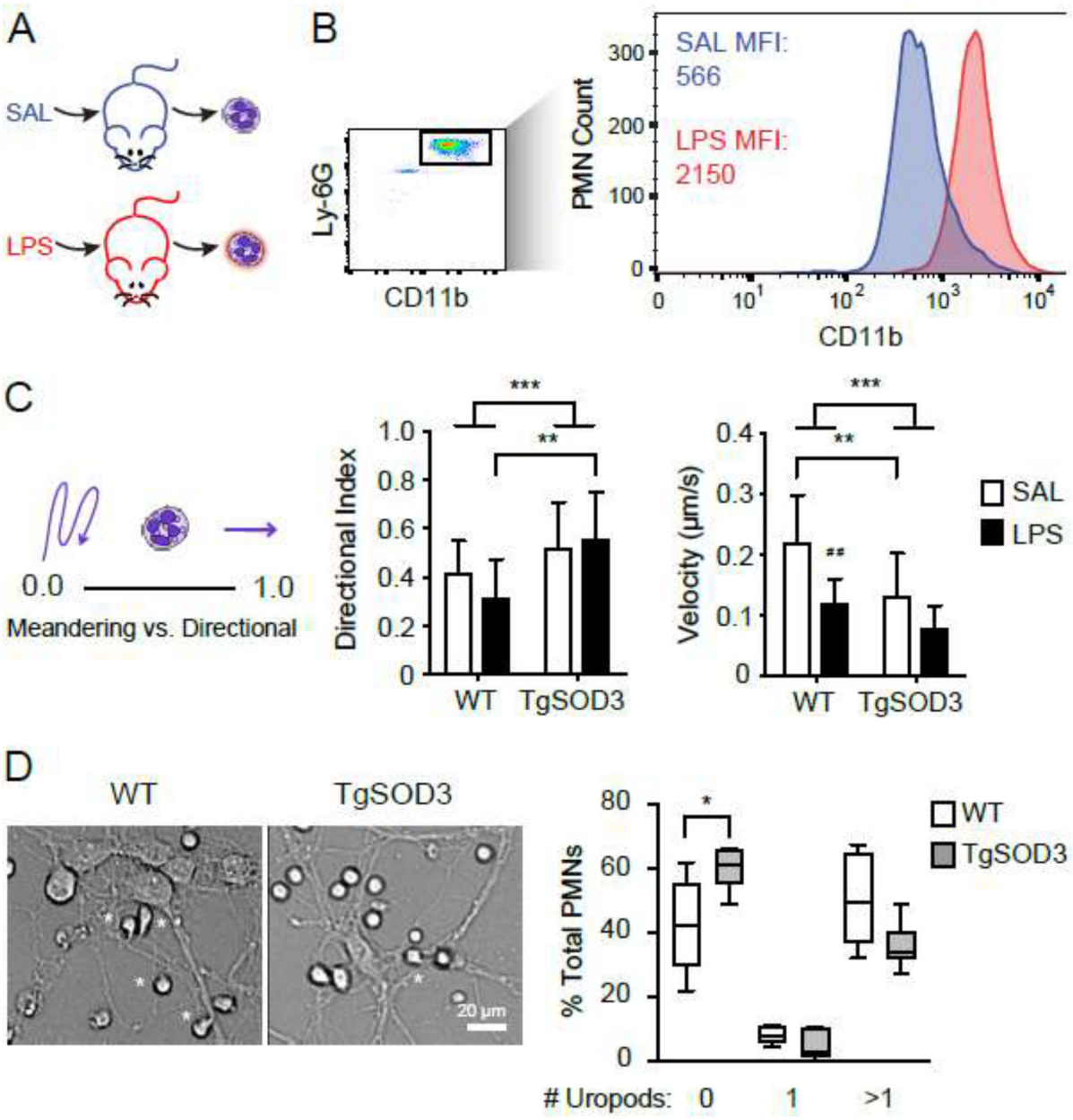

Figure 5.

In vitro PMN phenotyping. (A-B) WT and TgSOD3 mice were injected with saline or LPS for 6 hours, after which primed (LPS) and unprimed (SAL) Ly-6G^{hi}/CD11b^{hi} PMNs with distinct levels of CD11b expression were collected for neuron co-culture. (C) TgSOD3 PMNs traveled in a more linear path (higher directionality index) while WT PMNs meandered back and forth. TgSOD3 PMNs also traveled at lower velocities compared to WT PMNs, and LPS did not affect their speed (N = 12–21). (D) LPS-stimulated WT PMNs extended more uropods in interactions with neurons recovering from OGD (N = 6 individual fields per condition). Asterisks mark PMNs with uropods in contact with neuritic processes. Values represent means ± SD; * $p < 0.05$, ** $p < 0.01$, *** $p < 0.001$ between WT and TgSOD3; $^{\#\#}$ $p < 0.01$ between SAL and LPS.

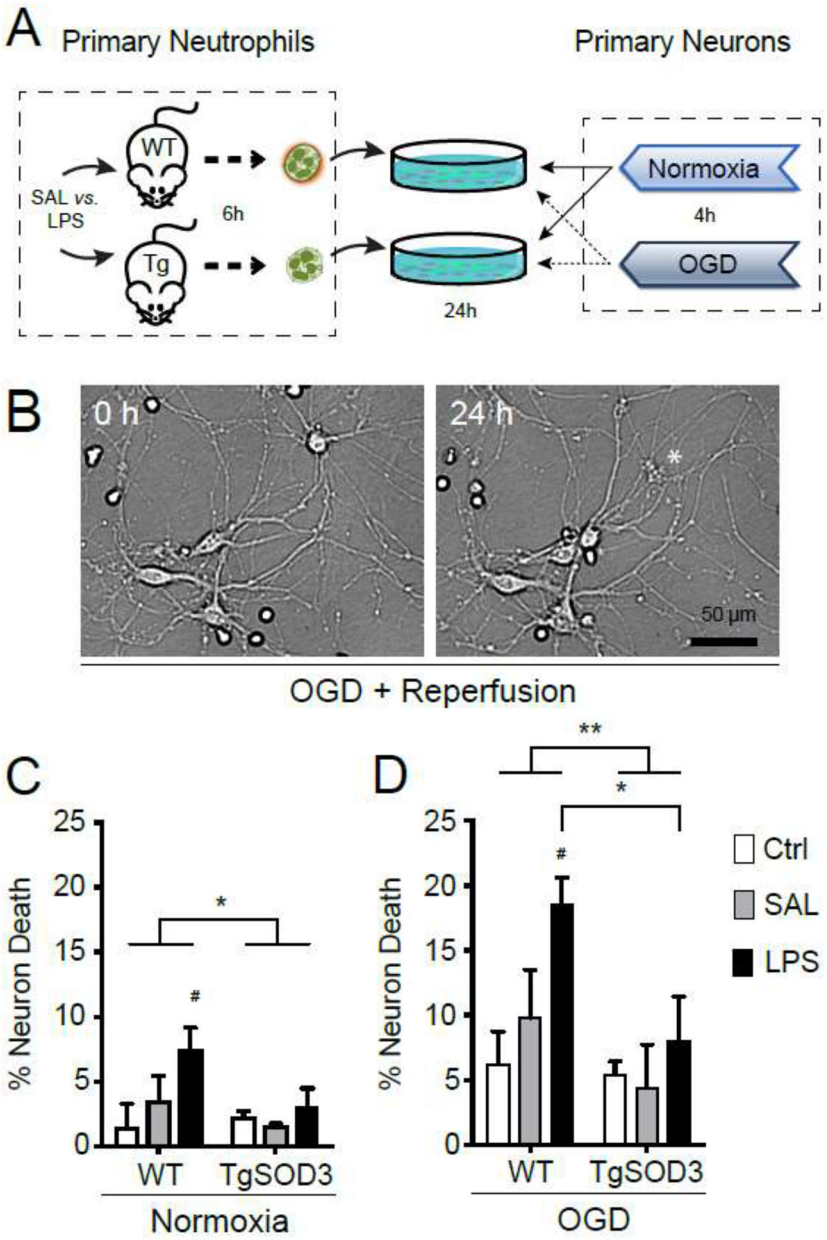

Figure 6.

PMNs from TgSOD3 donor mice exhibit reduced toxicity in primary neuronal cultures. (A) Six hours after IP injection with saline or LPS, PMNs were isolated from WT and TgSOD3 donor mice and co-cultured with control neurons or neurons recovering from 4-hour oxygen-glucose deprivation (OGD). (B) Brightfield images of primed PMN-neuronal co-cultures illustrating delayed neuronal rupture (asterisk) 24 hours after PMN treatment. (C) Effects of WT and TgSOD3 PMNs, ± donor lipopolysaccharide (LPS) priming, on neuron death in control cortical neuronal cultures, or (D) cortical neuronal cultures primed with sublethal OGD. Values represent means ± SD (n = 2–3 wells with >50 neurons analyzed per well). * *p*

< 0.05, ** $p < 0.01$ between WT and TgSOD3; # $p < 0.05$ between Ctrl (0 PMNs) and saline (SAL) or LPS-stimulated PMNs added at a 4:1 PMN:Neuron ratio.